New Phytologist

Terrestrial biosphere models underestimate photosynthetic capacity and CO_2 assimilation in the Arctic

Alistair Rogers[1], Shawn P. Serbin[1], Kim S. Ely[1], Victoria L. Sloan[2] and Stan D. Wullschleger[2]

[1]Environmental and Climate Sciences Department, Brookhaven National Laboratory, Upton, NY 11973-5000, USA; [2]Environmental Sciences Division, Oak Ridge National Laboratory, Oak Ridge, TN 37831-6301, USA

Author for correspondence:
Alistair Rogers
Tel: +1 631 344 2948
Email: arogers@bnl.gov

Received: *6 June 2017*
Accepted: *8 July 2017*

New Phytologist (2017) **216:** 1090–1103
doi: 10.1111/nph.14740

Key words: earth system models, maximum carboxylation capacity ($V_{c,max}$), maximum electron transport rate (J_{max}), photosynthesis, Rubisco, temperature response function, tundra.

Summary

- Terrestrial biosphere models (TBMs) are highly sensitive to model representation of photosynthesis, in particular the parameters maximum carboxylation rate and maximum electron transport rate at 25°C ($V_{c,max.25}$ and $J_{max.25}$, respectively). Many TBMs do not include representation of Arctic plants, and those that do rely on understanding and parameterization from temperate species.
- We measured photosynthetic CO_2 response curves and leaf nitrogen (N) content in species representing the dominant vascular plant functional types found on the coastal tundra near Barrow, Alaska.
- The activation energies associated with the temperature response functions of $V_{c,max}$ and J_{max} were 17% lower than commonly used values. When scaled to 25°C, $V_{c,max.25}$ and $J_{max.25}$ were two- to five-fold higher than the values used to parameterize current TBMs. This high photosynthetic capacity was attributable to a high leaf N content and the high fraction of N invested in Rubisco. Leaf-level modeling demonstrated that current parameterization of TBMs resulted in a two-fold underestimation of the capacity for leaf-level CO_2 assimilation in Arctic vegetation.
- This study highlights the poor representation of Arctic photosynthesis in TBMs, and provides the critical data necessary to improve our ability to project the response of the Arctic to global environmental change.

Introduction

Carbon (C) uptake and loss from high-latitude ecosystems are highly sensitive to climate change, and these processes are poorly represented in Earth system models. The Arctic has experienced the greatest regional warming (Kaufman *et al.*, 2009) and is projected to warm twice as much as the rest of the planet by the end of the century (IPCC, 2013). The resulting widely observed permafrost thaw and degradation are projected to continue as the region warms, leading to the release of large amounts of stored C into the atmosphere (Jorgenson *et al.*, 2006; Schuur *et al.*, 2009, 2015; Koven *et al.*, 2015). At the same time, rising carbon dioxide concentration ($[CO_2]$), increasing temperature and increased nitrogen (N) availability may stimulate CO_2 uptake and lead to a continued and enhanced 'greening' of the Arctic landscape, creating critical uncertainty over the future of the Arctic C cycle (Sturm *et al.*, 2001; Tape *et al.*, 2006; Frost & Epstein, 2014; Salmon *et al.*, 2016). Accurate projection of C fluxes at high latitudes will require improved model representation of these processes in terrestrial biosphere models (TBMs). A recent analysis has demonstrated that, in current TBMs, photosynthesis remains a dominant source of C cycle uncertainty in the Arctic (Fisher *et al.*, 2014).

Leaf-level photosynthesis is represented in many TBMs by the Farquhar, von Caemmerer and Berry (FvCB) model (Farquhar *et al.*, 1980; von Caemmerer, 2000). Two key parameters required by the FvCB model are the maximum carboxylation rate ($V_{c,max}$) by the photosynthetic enzyme Rubisco (EC number 4.1.1.39) and the maximum electron transport rate (J_{max}) associated with regeneration of the CO_2 acceptor molecule ribulose-1,5-bisphosphate (RuBP). Currently, most TBMs use plant functional types (PFTs) to represent the vegetation present in different biomes, and these PFTs are parameterized with traits that are used to model the CO_2 uptake of the vegetation in a given biome. There are a range of alternative approaches that seek to replace PFTs with a 'trait-based' approach in future TBMs (Wullschleger *et al.*, 2014). However, these approaches, such as trait–environment linkages (e.g. van Bodegom *et al.*, 2014), trait filtering (e.g. Fisher *et al.*, 2012) and optimality approaches (e.g. Xu *et al.*, 2012), still use an FvCB approach to represent photosynthesis, and still need data to inform parameterization, model development and to evaluate prognostic traits. In current TBMs, $V_{c,max}$ at 25°C ($V_{c,max.25}$) is typically a PFT-specific model input, whereas J_{max} at 25°C ($J_{max.25}$) is commonly calculated from the PFT-specific $V_{c,max.25}$ using a TBM-specific ratio between $J_{max.25}$ and $V_{c,max.25}$ ($JV_{ratio.25}$). The JV_{ratio} has also been used in the

opposite direction to estimate $V_{c,max}$ from remotely sensed chlorophyll content (Alton, 2017). Based on previous analysis (Wullschleger, 1993), $JV_{ratio.25}$ has long been assumed to be constant for all PFTs, but has been shown to decrease with increasing growth temperature (Kattge & Knorr, 2007). Critically, $JV_{ratio.25}$ can have a significant impact on photosynthetic CO_2 responsiveness, with a higher $JV_{ratio.25}$ enabling a more responsive Rubisco-limited increase in photosynthesis as [CO_2] rises (Rogers *et al.*, 2017c). In TBMs, photosynthesis is particularly sensitive to the temperature response functions (TRFs) used to scale both $V_{c,max}$ and J_{max} from the reference temperature, usually 25°C, to growth temperature. However, these TRFs are typically assumed to be identical for all PFTs (Rogers *et al.*, 2017c). Mounting evidence has shown that this is not a valid assumption and there is an ongoing effort in the community to capture PFT-specific TRFs for use in TBMs (Medlyn *et al.*, 2002; Varhammar *et al.*, 2015; Galmes *et al.*, 2016). This is particularly important for the Arctic, because widely used TRFs have been derived from measurements made on temperate species and do not include measurements made below 10°C, a typical growth temperature for Arctic species (Bernacchi *et al.*, 2001, 2003).

Sensitivity analysis, model simulations and efforts to identify model parameter uncertainty have repeatedly shown that model projections of gross and net primary productivity are particularly sensitive to $V_{c,max.25}$, and the parameters used to estimate it (Friend, 2010; Bonan *et al.*, 2011; Lebauer *et al.*, 2013; Sargsyan *et al.*, 2014). Moreover, previous studies have also shown that model uncertainty in plant productivity can be significantly reduced through the incorporation of PFT-specific measured values of $V_{c,max}$ (Dietze *et al.*, 2014). However, a recent examination of the derivation of $V_{c,max}$ in 10 TBMs revealed that most models do not have an explicit Arctic PFT and the four models that do include an Arctic PFT rely on limited or inappropriate datasets to estimate Arctic $V_{c,max.25}$ (Rogers, 2014).

There is a rich history of ecological research in the Arctic, including many studies that have measured photosynthesis (Wookey *et al.*, 1995; Chapin & Shaver, 1996; Muraoka *et al.*, 2002, 2008; Starr & Oberbauer, 2003; Starr *et al.*, 2004; Reich *et al.*, 2009; Albert *et al.*, 2011; Boesgaard *et al.*, 2012; Fletcher *et al.*, 2012; Leffler & Welker, 2013; Patankar *et al.*, 2013; Heskel *et al.*, 2014; Souther *et al.*, 2014; Saarinen *et al.*, 2016). However, at the time we began this study, there were no published data on $V_{c,max}$ or J_{max} measured in Arctic vegetation that could be used to inform the representation of Arctic photosynthesis in TBMs and, to the best of our knowledge, only one other study emerged after we began our work (van de Weg *et al.* 2013). In short, the data needed to understand and parameterize a key process that has been demonstrated to be driving marked uncertainty in TBM projections of the C cycle in a critical biome are essentially missing.

We hypothesized that current TBM representation and parameterization of photosynthesis, which is based largely on knowledge gained in temperate systems, will be markedly different for Arctic vegetation. The goal of this study was to increase our understanding of photosynthesis in the Arctic and to provide new data and insights that could be used to reduce uncertainty in TBM projections of photosynthesis in the Arctic, either directly through improved parameterization of the Arctic PFT, or indirectly through the evaluation of emergent model states that result from alternative 'trait-based' modeling approaches (prognostic photosynthetic parameters). In this study, we provide the first Arctic dataset on the critical photosynthetic traits $V_{c,max.25}$ and $J_{max.25}$, their TRFs and associated biochemical and structural traits; and compare these data with the parameterization currently used in TBMs, including the use of plant traits to derive photosynthetic parameters.

Materials and Methods

Plant material

This study was conducted on the coastal tundra at the Barrow Environmental Observatory (BEO), near Barrow, AK (71.3°N, 156.5°W; note that, on 1 December 2016, Barrow was officially renamed Utqiaġvik following the original Inupiat name), USA. The BEO landscape is characterized by small thaw ponds and low- and high-centered polygons with a low vascular plant species diversity that is dominated by *Carex aquatilis* (Brown *et al.*, 1980). Mean annual air temperature is −12°C (annual range, 31°C) and mean annual precipitation is 106 mm, with the majority falling as rain during the short summer. Soils are generally classified as Gelisols, underlain by permafrost which extends to depths of 300 m or greater, with an active layer thickness of 20–70 cm (Brown *et al.*, 1980; Bockheim *et al.*, 1999; Shiklomanov *et al.*, 2010).

The measurement of leaf traits and gas exchange was conducted over an area of *c.* 1 km^2 centered at 71.28°N, 156.65°W. This area was characterized by zones of disturbance and significant permafrost degradation, standing water, dry, high-centered polygons as well as relatively undisturbed low-centered polygonal ground that collectively provided diverse microtopography and drainage, and therefore highly suitable habitats for large stands of the different species of interest. Our goal was to measure key traits in the dominant vascular plants in this landscape, but also in those plants that represented key Arctic PFTs (Chapin *et al.*, 1996). Our choice of species was also constrained by practical limitations of the gas exchange instrumentation: for example, the ability to clamp on a leaf with sufficient leaf area to provide an acceptable signal-to-noise ratio that enabled us to measure a CO_2 response curve. We studied seven species covering four Arctic PFTs: grasses, *Arctagrostis latifolia* (R.Br.) Griseb, *Arctophila fulva* (Trin.) Andersson, *Dupontia fisheri* R.Br.; sedges, *Carex aquatilis* Wahlenb., *Eriophorum angustifolium* Honck.; forbs, *Petasites frigidus* (L.) Fr.; and deciduous shrubs, *Salix pulchra* Cham. As a result of the clonal nature of these species, it was not possible to determine whether individual ramets were genetically distinct. Therefore, stands separated by geomorphological features, i.e. different polygonal units or thaw ponds, were chosen to increase the likelihood that they were not members of the same clonal colony (Shaver *et al.*, 1979). Measurements were taken between 10 July and 10 August (2012–2016), a period characterized by cool temperatures and continuous daylight. The bulk of

our measurements were focused on the period of the peak biomass (mid to late July), when the first mature leaves in these species are available for gas exchange, but before the onset of leaf senescence. As a result of the scarcity of individuals of some species (*S. pulchra*), additional data collection associated an effort to link leaf spectral signatures with physiology (Serbin *et al.*, 2012) and the challenge of taking good measurements (*D. fisheri*), our replication within a species varied (*A. latifolia*, $n = 13$; *A. fulva*, $n = 26$; *C. aquatilis*, $n = 36$; *D. fisheri*, $n = 8$; *E. angustifolium*, $n = 43$; *P. frigidus*, $n = 44$; *S. pulchra*, $n = 9$).

Gas exchange and derived parameters

Gas exchange measurements were made in the field using two to five LI-6400XT gas exchange systems (Li-Cor, Lincoln, NE, USA) that were zeroed at the field site with a common nitrogen standard (99.9998% N_2, $CO_2 < 0.5$ ppm, $H_2O < 0.5$ ppm; Alphagaz 2, Air Liquide American Specialty Gases LLC, Anchorage, AK, USA). We measured the response of photosynthesis (A) to intercellular CO_2 concentration (C_i), commonly called A–C_i curves. Leaf chamber temperature was maintained at ambient temperature using the Peltier-based temperature control of the gas exchange system by setting the chamber block temperature to match the air temperature measured using the leaf thermocouple with the chamber open. The water vapor pressure of air entering the chamber was not controlled and therefore matched ambient conditions. However, on cold, high-humidity days, the block temperature was set to 0.5–1.5°C above ambient air temperature to increase the differential between the dew point temperature and the chamber block temperature in order to eliminate the chance of condensation inside the instrument. Even with this slight increase in temperature, the leaf water vapor pressure deficit (VPD_{leaf}) was always below 1.0 kPa and, typically, *c.* 0.3 kPa. All measurements were made on fully expanded leaves. When the leaf did not completely fill the leaf chamber of the instrument, which was the case for all the graminoid species, the leaf material protruding from the chamber was marked at the edge of the gasket to identify the section that was enclosed in the chamber. The leaf was then removed from the chamber and plant, and the enclosed section was measured indoors with a ruler and hand lens to allow the determination of the leaf width to the nearest 0.25 mm. The leaf width was then used to calculate the leaf area enclosed by the leaf chamber, and gas exchange data were recomputed using the measured leaf area.

During the period of measurement, the Arctic experiences 24 h of daylight. As a result, transient decreases in chloroplast inorganic phosphate concentration and photosystem II efficiency, which can occur shortly after initial illumination, and which may alter the response of A to C_i, are not a concern (Ainsworth *et al.*, 2003). In addition, attempts to remove plant material from the field and to conduct measurements indoors, where marked temperature manipulation would be possible, were unsuccessful. Therefore, A–C_i curves were all measured *in situ*. Preliminary light response curves, in which we carefully controlled for CO_2 concentration and leaf temperature, indicated that, despite expectations, these Arctic species did not photosaturate below 1500 $\mu mol\ m^{-2}\ s^{-1}$. Therefore, we used an irradiance of 2000 $\mu mol\ m^{-2}\ s^{-1}$ for our light-saturated measurements. The differential between sample and reference infrared gas analyzers (IRGAs) was maximized using the 2×3-cm^2 leaf chamber to increase potential leaf area, and by lowering the flow rate (typically to 350 $\mu mol\ s^{-1}$) until the CO_2 differential between sample and reference chambers was *c.* 10 $\mu mol\ CO_2\ mol^{-1}$ at a CO_2 reference chamber set point of 400 $\mu mol\ mol^{-1}$ and saturating irradiance. This ensured a good signal-to-noise ratio at low $[CO_2]$. After clamping on a leaf, the chamber was leak tested by vigorously blowing through a tube directed at the margins of the gasket. When leaks were identified (fluctuations in $[CO_2]$ in the sample cell > 1 $\mu mol\ mol^{-1}$ over 15 s), the leaf was repositioned or leaks were sealed with a silicone compound (Molykote 111; Dow Corning, MI, USA). Following the established procedure (Long & Bernacchi, 2003; Bernacchi *et al.*, 2006), each leaf was first allowed to achieve steady-state CO_2 and water vapor exchange. The minimum amount of time allowed for stabilization was 20 min, but, typically, we waited more than 30 min. The reference $[CO_2]$ was then reduced stepwise to 50 $\mu mol\ mol^{-1}$, returned to 400 $\mu mol\ mol^{-1}$ and then increased stepwise to 1800 $\mu mol\ mol^{-1}$. Each individual curve consisted of 13 separate CO_2 set points and included multiple set points at a $[CO_2]$ value of 400 $\mu mol\ mol^{-1}$ to allow for potential recovery from low $[CO_2]$. Response curves were measured rapidly to avoid acclimation to a given set point. Following an adjustment to a new $[CO_2]$ value, data were logged as soon as the $[CO_2]$ in the reference cell was stable (SD < 0.75 $\mu mol\ mol^{-1}$ over 20 s). Following equilibration, each curve took *c.* 30 min to complete.

In addition to making measurements at ambient growth temperature in all species, we also measured A–C_i response curves at multiple temperatures on the same leaf in *P. frigidus* and *E. angustifolium* in order to expand the temperature range of our dataset. This was achieved using the cooling and heating feature of the gas exchange system. In some cases, we focused on the initial slope of this response to speed up measurements and, as a result, collected more data on the temperature response of $V_{c,max}$ than J_{max}. In each case, following the completion of a full or partial CO_2 response curve, the leaf temperature was increased by *c.* 5°C and allowed to stabilize for a minimum of 20 min before a new response curve was measured. At our high-temperature limit (25°C), VPD_{leaf} did not rise above 1.75 kPa. Analysis of the data from a nearby flux tower (Torn *et al.*, 2014 and unpublished data) showed that mean daily air temperatures on the days preceding our measurements were similar (3.7 ± 2.5 SD (5-d average), 4.3 ± 2.0 SD (10-d average), 4.3 ± 1.7 SD (30-d average)), giving us confidence that, when combining our full dataset for the analysis of temperature response functions, there would be no marked impact of potential thermal acclimation to the air temperature of the days preceding our measurements.

The photosynthetic parameters $V_{c,max}$ and J_{max} were estimated based on the equations originally described by Farquhar *et al.* (1980), where A is the minimum of the RuBP-saturated CO_2

assimilation rate (A_c) and the RuBP-limited CO_2 assimilation rate (A_j, Eqn 1).

$$A = \min(A_c, A_j) \quad \text{Eqn 1}$$

Triose phosphate utilization (TPU) limitation can also be a third limitation on A, but usually occurs at a higher than physiologically relevant CO_2 concentration (Sharkey, 1985). We saw no evidence of TPU limitation of A in our A–C_i curves, despite the low measurement temperatures. One possible explanation for the absence of TPU limitation is the large root : shoot ratio (Iversen *et al.*, 2015), and hence sink capacity, in Arctic species which would limit the potential feedback inhibition of photosynthesis by minimizing the buildup of triose phosphate in the leaves. Therefore, we did not include TPU limitation in our model formulation for the estimation of $V_{c,max}$ and J_{max}. We did not account for the influence of mesophyll conductance on the estimates of $V_{c,max}$ and J_{max}, and thus our reported 'apparent' values are based on intercellular as opposed to chloroplastic $[CO_2]$.

Apparent $V_{c,max}$ and apparent J_{max} were determined based on C_i, as described previously, using the commonly employed method of separate fitting of A to C_i for Rubisco and RuBP regeneration-limited A (Farquhar *et al.*, 1980; Bernacchi *et al.*, 2013). A_c was modeled based on Eqn 2, where C_i and O_i are the intercellular CO_2 and O_2 concentrations ($O_i = 210$ mmol mol^{-1}), respectively, Γ^* is the CO_2 compensation point in the absence of non-photorespiratory mitochondrial respiration in the light, and K_c and K_o are the Michaelis–Menten coefficients of Rubisco activity for CO_2 and O_2, respectively. We used the NADPH-limited version of the equation used to describe the electron transport rate in the determination of the RuBP-limited CO_2 assimilation rate (A_j, Eqn 3), and employed the values and temperature sensitivities of K_c, K_o and Γ^* from Bernacchi *et al.* (2001).

$$A_c = \frac{(C_i - \Gamma^*)V_{c,max}}{K_c\left(1 + \frac{O_i}{K_o}\right) + C_i} - R_d \quad \text{Eqn 2}$$

$$A_j = \frac{(C_i - \Gamma^*)J}{4C + 8\Gamma^*} - R_d \quad \text{Eqn 3}$$

We parameterized Eqns 2 and 3 of the FvCB model, using a custom program (https://github.com/TESTgroup-BNL/R-GasExchange/releases/tag/0.8) developed within the R statistical environment (R Development Core Team, 2013), to calculate the optimum apparent $V_{c,max}$, apparent J_{max} and leaf respiration for each A–C_i curve. Our model fitting utilized the derivative evolution (DE) algorithm (Price *et al.*, 2006), implemented in the R package 'DEoptim' (Ardia, 2009), to minimize the difference between the modeled and observed photosynthetic rate to derive the optimum apparent $V_{c,max}$ and apparent J_{max} for each A–C_i curve. The DE algorithm is a stochastic, population-based optimizer, which seeks the global minimum of the objective function without the need for arbitrary initial parameter values which can result in errors in optimization (Dubois *et al.*, 2007). Our parameter optimization strategy was implemented to avoid the co-limited region of the A–C_i response curve, which, for these Arctic species, was at a high C_i: $V_{c,max}$ was estimated from the lower portion of the A–C_i curve ($C_i < 400$ Pa) and J_{max} was estimated from the upper portion of the curve ($C_i > 650$ Pa).

The temperature responses of $V_{c,max}$ and J_{max} were determined by fitting measured values against the mean T_{leaf} for each individual A–C_i response curve, as described previously (Medlyn *et al.*, 2002), which allowed us to estimate the activation energy (E_a) associated with $V_{c,max}$ and J_{max}. We then used Eqn 4 (shown for $V_{c,max}$) to scale the measured $V_{c,max}$ at T_{leaf} ($V_{c,max.T}$) to $V_{c,max}$ at 25°C ($V_{c,max.25}$). T_{leaf} was expressed in K and R is the universal gas constant (8.314 J mol^{-1} K^{-1}). Again, we utilized the 'DEoptim' parameter optimization algorithm in R to fit the temperature response model (Eqn. 4).

$$V_{c,max.T} = V_{c,max.25} \exp\left[\frac{E_a(T_{leaf} - 298.15)}{(298.15R\,T_{leaf})}\right] \quad \text{Eqn 4}$$

Biochemical analysis

The leaf area enclosed by the leaf chamber of the IRGA was removed, placed in a paper envelope and dried to a constant mass (70°C, Lindberg Blue M, Thermo Scientific, Waltham MA, USA) before shipping to Brookhaven National Laboratory. Leaf samples were weighed to obtain the leaf mass area (LMA, g m^{-2}) and then ground to a fine powder using a ball mill (2000 Geno Grinder; Spex Sample Prep, Cridersville, OH, USA). A 1.50–2.50-mg aliquot was weighed in 0.1-ml tin foil vials (AX26DR; Mettler Toledo, Columbus, OH, USA) and used to determine the C to N ratio (CN_{ratio}) and elemental N content employing a CHNS/O elemental analyzer operated in CHN mode, according to the manufacturer's instructions (2400 Series II CHNS/0 Analyzer; Perkin Elmer, Waltham, MA, USA).

The fraction of leaf N invested in Rubisco

The fraction of leaf N invested in Rubisco (F_{LNR}) can be calculated as described previously (Thornton & Zimmermann, 2007) following Eqn 5, where leaf N content on an area basis (N_a, g m^{-2}) and $V_{c,max.25}$ are PFT-specific inputs, and the specific activity of Rubisco (α_{R25}) and the mass ratio of total Rubisco molecular mass to N in Rubisco (F_{NR}) are considered to be global constants.

$$F_{LNR} = \frac{V_{c,max.25}}{N_a F_{NR} \alpha_{R25}} \quad \text{Eqn 5}$$

We derived F_{LNR} from the mean $V_{c,max.25}$ (Fig. 2a), mean N_a (Fig. 4a) and the values for F_{NR} (6.22 g Rubisco g^{-1} N in Rubisco) and α_{R25} (47.3 μmol CO_2 g^{-1} Rubisco s^{-1}) provided by Rogers (2014).

Models considered

We looked at the model parameterization for all the TBMs represented in the fourth and fifth phases of the Coupled Climate Carbon Cycle Model Intercomparison Project (Friedlingstein *et al.*, 2006, 2014) and those identified in a recent review of global scale models (Smith & Dukes, 2013). Only four models included explicit parameterization of an Arctic PFT and were considered in detail here (Table 1). In order to compare the parameterization of these four models with the data presented in this study and, importantly, to avoid mixing and matching temperature response functions and kinetic constants (Rogers *et al.*, 2017c), we scaled our measured photosynthetic parameters to 25°C using the temperature response functions and Q_{10} values or activation energies for $V_{c,max}$ and J_{max} used by the models (Table 1). For the Atmosphere–Vegetation Interaction Model (AVIM), it was necessary to refit the A–C_i response curves using the kinetic constants and TRFs employed by Collatz *et al.* (1991), and then scale $V_{c,max.T}$ to 25°C using the Q_{10} temperature response function for AVIM presented in Table 1. To account for the temperature acclimation formulations in the Biosphere Energy Transfer Hydrology Scheme (BETHY) and Community Land Model (CLM) used in the calculation of $JV_{ratio.25}$ and ΔS (Table 1), we employed data from a nearby flux tower to provide mean daily air temperature for the proceeding 10 (CLM) and 30 (BETHY) days. For CLM, this 10-d mean temperature was below the restricted temperature range implemented in the model, and therefore the 11°C default value was used in our calculations (Oleson *et al.*, 2013).

Statistical analysis

Significant ($P < 0.05$) variation among species was identified using a one-way analysis of variance (ANOVA). Significant differences between an individual species (or the seven species mean) and an individual TBM input were identified using a one-sample *t*-test. Significant differences between the measured photosynthetic parameters and the model inputs from the four TBMs, and differences between the leaf-level photosynthesis modeled with the measured parameterization and TBM parameterization, were identified using a two-tailed Student's *t*-test.

Results

Activation energy values associated with the temperature response functions of $V_{c,max}$ and J_{max}

Fitting an Arrhenius temperature response function (Eqn 4, Fig. 1) to our full datasets of $V_{c,max.T}$ and $J_{max.T}$ showed that the derived E_a values associated with the temperature response functions of $V_{c,max}$ and J_{max} were *c.* 17% lower than the values reported by Bernacchi *et al.* (2001, 2003). If the E_a values derived by Bernacchi *et al.* (2001) were used to scale model inputs of $V_{c,max.25}$ and $J_{max.25}$ values to a typical Arctic growth temperature (5°C), $V_{c,max}$ and J_{max} would be underestimated by *c.* 25%. Similarly scaling our measured values to 25°C using our E_a values would result in a lower $V_{c,max.25}$ and $J_{max.25}$ than if those same values were scaled to 25°C using the TRFs of Bernacchi *et al.* (2001, 2003). Therefore, we used the E_a values determined in this study (Fig. 1) to scale our data to a common reference temperature of 25°C. Values of E_a generated from small species-specific datasets, or datasets with a limited temperature range, have the potential to introduce additional sources of uncertainty. Therefore, we adopted the community-level E_a values presented in Fig. 1 rather than use species-specific E_a values.

Photosynthetic traits and key model inputs

Estimates of the key TBM inputs, apparent $V_{c,max.25}$ and apparent $J_{max.25}$ (Fig. 2a,b), were determined from A–C_i response curves made at growth temperature and scaled to 25°C using the temperature response function shown in Eqn 4 and the E_a values for $V_{c,max}$ and J_{max} determined in this study (Fig. 1). These values were used to calculate the apparent JV_{ratio} at 25°C ($JV_{ratio.25}$, Fig. 2c). Apparent mean $V_{c,max.25}$ (Fig. 2a) showed significant ($F_{6,173} = 19.2$, $P < 0.001$) variation between species, ranging from 69 μmol m^{-2} s^{-1} in *D. fisheri* to 113 μmol m^{-2} s^{-1} in *A. fulva*. Apparent $JV_{ratio.25}$ did not differ significantly between species ($F_{6,142} = 1.9$, $P = 0.08$, Fig. 2c), and therefore species variation in apparent $J_{max.25}$ mirrored apparent $V_{c,max.25}$, ranging from 183 μmol m^{-2} s^{-1} in *D. fisheri* to 297 μmol m^{-2} s^{-1} in *A. fulva* ($F_{6,142} = 14.4$, $P < 0.001$, Fig. 2b). In order to compare the shape of the A–C_i curves between species that were measured at a range of temperatures, we modeled the response of A to C_i at two leaf temperatures (5 and 15°C) using Eqns 1–3 and the mean species-specific values for $V_{c,max.25}$ and $J_{max.25}$ presented here (Fig. 2a,b). In all seven species at both 5°C (Fig. 3a) and 15°C (Fig. 3b), photosynthesis was Rubisco limited (RuBP saturated) at current [CO_2]. At 5°C, photosynthesis was Rubisco limited throughout the A–C_i curve. Even at 15°C, photosynthesis did not become RuBP limited in any species until the atmospheric CO_2 concentration reached *c.* 785 μmol mol^{-1} (a C_i of *c.* 550 μmol mol^{-1}, Fig. 3b).

Leaf N content (N_a, Fig. 4a), calculated from the leaf mass area (LMA, Fig. 4b) and mass-based N content (N_m, data not shown), also varied significantly between species ($F_{6,151} = 37.6$, $P < 0.001$), but did not show the same pattern as $V_{c,max.25}$ or $J_{max.25}$. The LMA and CN_{ratio} (Fig. 4c) both varied significantly between species (LMA, $F_{6,162} = 40.4$, $P < 0.001$; CN_{ratio}, $F_{6,153} = 64$, $P < 0.001$). Our paired gas exchange and N_a dataset allowed us to calculate F_{LNR} (Fig. 5), which varied significantly between species ($F_{6,156} = 80$, $P < 0.001$) and was notably high in *A. fulva*, where 34% of leaf N was invested in Rubisco.

$V_{c,max}$–leaf N relationship

We found no clear relationship between apparent $V_{c,max.25}$ and N_a (Fig. 6). We doubled the size of our $V_{c,max}$–N_a dataset by leveraging estimates of apparent $V_{c,max.25}$ derived from an additional dataset of light-saturated A (A_{sat}) using the one-point method for the estimation of $V_{c,max.25}$ (De Kauwe *et al.*, 2016) and coupled measurements of N_m and LMA. When we included the derived apparent $V_{c,max\cdot25}$ and N_a data in our analysis, we

Table 1 Parameters and equations used by the four terrestrial biosphere models (TBMs) that include an Arctic plant functional type (PFT); the Atmosphere–Vegetation Interaction Model (AVIM), the Biosphere Energy Transfer Hydrology Scheme (BETHY), the Community Land Model v4.5 (CLM4.5) and Hybrid version 6.5 (Hybrid6.5)

	AVIM	BETHY	CLM4.5	Hybrid6.5
Form of FvCB model	$A = (A_c, A_j) - R_d$ Collatz *et al.* (1991)	$A = (A_c, A_j) - R_d$	$A = (A_c, A_j, A_p) - R_d$	$A = (A_c, A_j) - R_d$ Kull & Kruijt (1998)
$V_{c,max.25}$ (μmol m^{-2} s^{-1})	55	20	78	37
Temperature acclimation of $JV_{ratio.25}$ (source)	NA	$JV_{ratio.25} = 2.59 - 0.035(T_g - T_f)$ In CLM, acclimation to low temperature is restricted where $(T_g - T_f) \geq 11$°K Kattge & Knorr (2007)		NA
$JV_{ratio.25.Tg}$	NA	2.44	2.21	NA
$J_{max.25}$ (μmol m^{-2} s^{-1})	NA	49	172	209*
Source of kinetic constants	Collatz *et al.* (1991)	Bernacchi *et al.* (2001, 2003), Kattge & Knorr (2007)	Bernacchi *et al.* (2001, 2003), Kattge & Knorr (2007)	Bernacchi *et al.* (2001), Friend (1995)
Temperature response functions	$V_{c,max} = V_{c,max.25} Q_{10}^{\frac{(T_{leaf}-25)}{10}}$	$V_{c,max} = V_{c,max.25} \exp\left(E_a \frac{T_{leaf}-298.15}{298.15 R T_{leaf}}\right) \frac{1+\exp\left(\frac{298.15\Delta S - E_d}{298.15R}\right)}{1+\exp\left(\frac{T_{leaf}\Delta S - E_d}{T_{leaf}R}\right)}$ $\Delta S = 668.39 - 1.07(T_g - T_f)$ In CLM, acclimation to low temperature is restricted where $(T_g - T_f) \geq 11$ Kattge & Knorr (2007)		$V_{c,max} = \exp\left(\frac{c - E_a}{R T_{leaf}}\right)$ $j_{max} = \frac{\alpha_T \exp\left(\frac{-E_a}{R T_{leaf}}\right)}{1+\exp\left[\frac{(\Delta S T_{leaf} - E_d)}{R T_{leaf}}\right]}$
Temperature response parameters for $V_{c,max}$	$Q_{10} = 2.4$	$E_a = 71.510$ kJ mol^{-1} $E_d = 200$ kJ mol^{-1} $\Delta S = 650$ J K^{-1} mol^{-1}	$E_a = 72$ kJ mol^{-1} $E_d = 200$ kJ mol^{-1}	$E_a = 65.33$ kJ mol^{-1} $c = 26.35$
Temperature response parameters for J_{max}	NA	NA	NA	$\alpha_T = 3.486 \times 10^{13}$ mol mol^{-1} s^{-1} $E_a = 79.5$ kJ mol^{-1} $E_d = 199$ kJ mol^{-1} $\Delta S = 650$ J K^{-1} mol^{-1}
CN_{ratio}	NA	NA	25	NA
N_a (g m^{-2})	NA	NA	1.3	1.6
Apparent F_{LNR}	NA	NA	0.1365	0.078
Key model reference	Lu & Ji (2006)	Ziehn *et al.* (2011)	Oleson *et al.* (2013)	Friend & Kiang (2005)

A, CO_2 assimilation rate; A_c, RuBP saturated CO_2 assimilation; A_j, RuBP limited CO_2 assimilation rate; A_p, triose phosphate export limited rate of CO_2 assimilation; T_g, the preceding 10 d (CLM, 4.25°C) and 30 d (BETHY, 4.28°C) mean air temperature (°K) calculated in this study from data from a nearby flux tower (Torn *et al.*, 2014); T_f, freezing point of water (°K); $JV_{ratio.25.Tg}$, $JV_{ratio.25}$ acclimated to growth temperature; E_a, activation energy; E_d, deactivation energy; R, universal gas constant; ΔS, entropy factor; j_{max}, light saturated potential electron transport (mol electrons mol^{-1} chlorophyll s^{-1}) rate; α_T, a constant linking electron to chlorophyll content. *J_{max} was calculated from j_{max} as described previously (Friend, 1995). Apparent F_{LNR} for Hybrid6.5 was calculated from N_a and $V_{c,max.25}$ based on Rogers (2014). NA, not applicable.

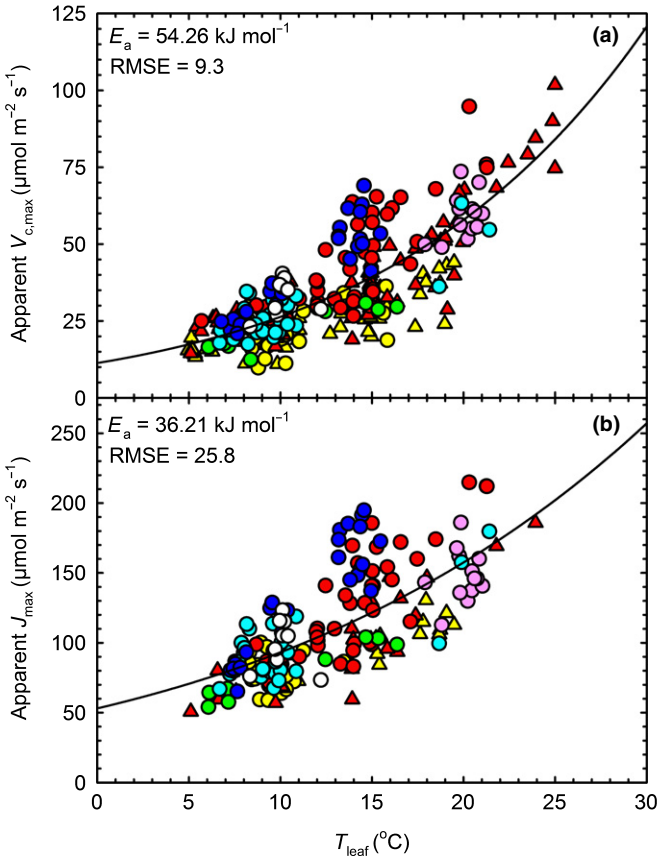

Fig. 1 Apparent maximum carboxylation rate ($V_{c,max}$, a) and apparent maximum electron transport rate (J_{max}, b) measured on individual ramets at ambient growth temperature (circles, seven species) and at multiple leaf temperatures on the same ramet (upward pointing triangles, two species) in *Arctagrostis latifolia* (pink), *Dupontia fisheri* (green), *Arctophila fulva* (blue), *Carex aquatilis* (cyan), *Eriophorum angustifolium* (yellow), *Petasites frigidus* (red) and *Salix pulchra* (white) growing on the Barrow Environmental Observatory, Barrow, Alaska. An Arrhenius temperature response (black line) was fitted to the data in order to calculate an activation energy (E_a) for both $V_{c,max}$ and J_{max}.

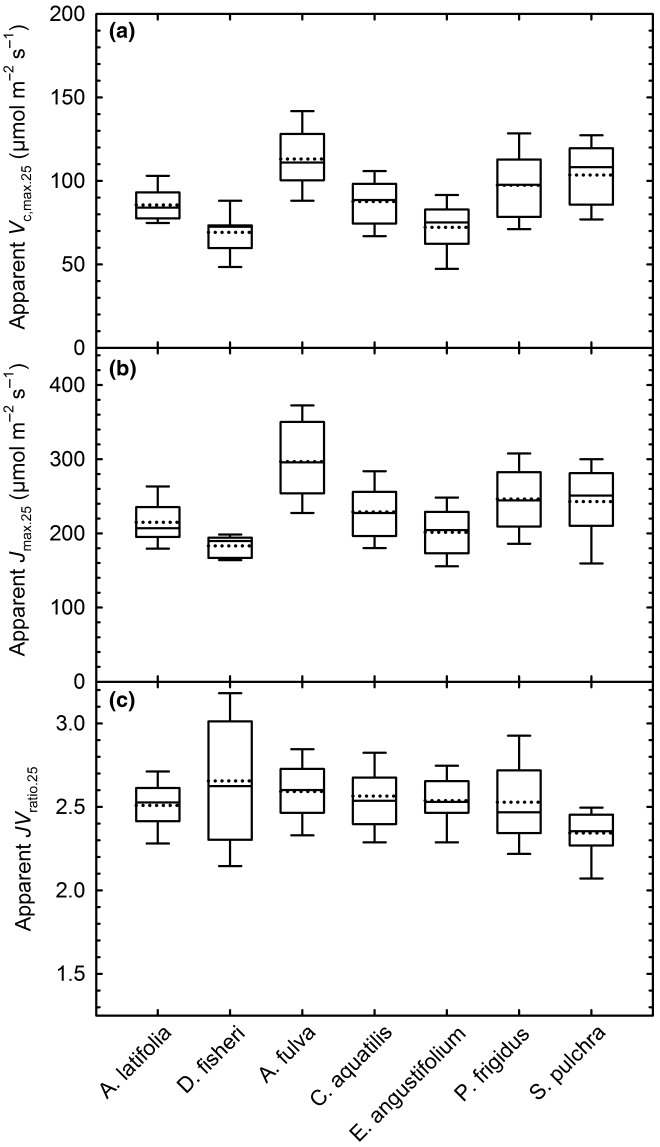

Fig. 2 Apparent maximum carboxylation rate ($V_{c,max.25}$, a) and apparent maximum electron transport rate ($J_{max.25}$, b) scaled to 25°C using the E_a values determined from the temperature response of $V_{c,max}$ and J_{max} presented in Fig. 1, and the ratio of $J_{max.25}$ to $V_{c,max.25}$ ($JV_{ratio.25}$, c). Data were measured in seven species located on the Barrow Environmental Observatory, Barrow Alaska. All data presented in this figure were derived from measurements made at ambient temperature. Box plots show the interquartile range (box), median (solid line) and mean (broken line). The whiskers show the lowest and highest datum still within 1.5 × interquartile range of the lower and upper quartiles (n = 8–44 plants).

still found that N_a could explain no more than 2% of the variation in $V_{c,max.25}$ (Fig. 6).

Comparison with TBM parameterization

To enable fair comparison of the gas exchange data presented here with the model parameterization in the four TBMs considered, we scaled our data from growth temperature to 25°C using model-specific temperature response functions and parameterization (Table 1). All four models markedly and significantly (one-sample t-tests, $P < 0.05$) underestimated $V_{c,max.25}$ in all seven species (Fig. 7), ranging from CLM (Fig. 7c, long dashes), where the model parameterization was 42% lower than the seven species mean, to BETHY (Fig. 7b), where the model parameterization was five times lower than the seven species mean. The model comparison with measured $J_{max.25}$ (Fig. 8) shows that, for BETHY (Fig. 8a) and CLM (Fig. 8b), $J_{max.25}$ was markedly and significantly higher than the model parameterization: 55% higher in CLM (Fig. 8b) and over five-fold higher in BETHY (Fig. 8a; Table 1). In TBMs, $J_{max.25}$ is typically calculated from the model estimate of $V_{c,max.25}$ and $JV_{ratio.25}$. The species mean $JV_{ratio.25}$ (2.53 ± 0.04 SE, Fig. 2c) is 4% and 13% higher than $JV_{ratio.25}$ used by BETHY (2.44) and CLM (2.21), respectively (one-sample t-tests, $P < 0.05$, Fig. 2c, Table 1). The use of our Arctic E_a values resulted in a small (*c.* 10%), but significant ($t_{(6)} = 8.1$, $P < 0.001$), increase in the observed $JV_{ratio.25}$ when compared with the $JV_{ratio.25}$ that would have been obtained using the E_a values provided by Bernacchi *et al.* (2001, 2003). The Hybrid model uses a different approach to estimate $J_{max.25}$ based on N_a

(Table 1); as a result, the pattern of derived $J_{max.25}$ for Hybrid follows that of N_a (Fig. 4a). The Hybrid $J_{max.25}$ estimate was significantly higher than *A. latifolia*, *D. fisheri* and *A. fulva*, but significantly lower than *C. aquatilis*, *E. angustifolium*, *P. frigidus* and *S. pulchra* (one-sample *t*-tests, $P < 0.05$).

Model parameterization associated with leaf chemistry more closely matched the observations. For N_a, the seven-species mean was not significantly different from the value used by Hybrid (Fig. 4a, short dashes), but was significantly (one-sample $t_{(6)} = 2.1$, $P < 0.05$) higher than the mean used by CLM (Fig. 4a, long dashes). CLM also uses CN_{ratio} as a model input and the seven-species mean was 23% lower than the CLM value (one-sample $t_{(6)} = 2.4$, $P > 0.05$). With the exception of *E. angustifolium*, all species had a higher investment in Rubisco than that prescribed by CLM, and the seven-species mean was *c.* 30% higher than the model input (one sample $t_{(6)} = 2.1$, $P < 0.05$, Fig. 5, long dashed line). The F_{LNR} value calculated for Hybrid was 60% lower than the observed seven-species mean (Fig. 5, short dashed line).

Comparison of modeled and measured CO_2 assimilation

To evaluate the effect of these new data on the modeled CO_2 uptake in the Arctic, we compared model estimates for light-saturated leaf-level A at 5°C modeled with the TBM-specific parameterization and TRFs (Table 1) with the data presented here (Figs 1, 2). The mean observed $V_{c,max.5}$ was more than twice the TBM model mean $V_{c,max.5}$ ($t_{(5)} = 4.6$, $P < 0.01$, Table 2), and the resulting species mean A modeled using our parameterization and TRF was 2.5 times greater than the A value modeled with current TBM parameterization ($t_{(5)} = 4.6$, $P < 0.01$, Table 2).

As an additional step, we compared our modeled data with independent measurements of light-saturated A made in the field at 5°C in 2016. These data showed that A modeled with the mean TBM parameterization of $V_{c,max.25}$ resulted in a CO_2 uptake rate that was less than half the measured CO_2 assimilation rate ($t_{(3)} = 3.7$, $P < 0.05$). A modeled with the parameter values determined by this study was *c.* 20% higher than the measured values, but not significantly different ($t_{(9)} = 2.2$, $P > 0.05$) from A measured in 2016.

Discussion

We have shown that TBM representation of photosynthetic capacity in Arctic vegetation markedly underestimates the capacity for CO_2 assimilation in this globally important biome. Our data showed that the photosynthetic capacity was high (Fig. 2) – all seven species had values for $V_{c,max.25}$ that were comparable with, or higher than, those found in major C3 crops (Bernacchi *et al.*, 2005; James *et al.*, 2006; Zhu *et al.*, 2012) – and up to five times higher than some model estimates (Fig. 7). Leaf-level modeling demonstrated that current TBM parameterization of photosynthetic capacity results in a two-fold underestimation of CO_2 assimilation by Arctic vegetation (Table 2). This study provides one of the first datasets of the key photosynthetic parameters $V_{c,max}$ and J_{max} in Arctic vegetation and the first estimates of their TRFs (Figs 1, 2). Our data also showed that model underestimation of photosynthetic capacity is attributable to a combination of low estimates of the leaf N content (Fig. 4) and the fraction of N partitioned to Rubisco (Fig. 5).

The JV_{ratio} affects the CO_2 responsiveness of A, such that a high JV_{ratio} will mean that A remains RuBP saturated at a high $[CO_2]$, and is therefore more responsive to increasing $[CO_2]$, than RuBP limited A in a plant with a lower JV_{ratio} (Rogers *et al.*, 2017c). The result of the high JV_{ratio} in these Arctic species can be readily seen in Fig. 3b, where, even at 15°C, A does not become RuBP limited in any species until a C_i value of *c.* 550 µmol mol^{-1}. This means that Arctic vegetation has the potential to respond maximally to rising $[CO_2]$ through most of this century. The high investment in Rubisco, coupled with the high $JV_{ratio.25}$, enables plants growing at current $[CO_2]$ to sustain high, RuBP-saturated, photosynthetic rates, even at low temperature and low light levels.

The high JV_{ratio} will also enable Arctic plants to continue CO_2 assimilation during the continuous but lower irradiance of the

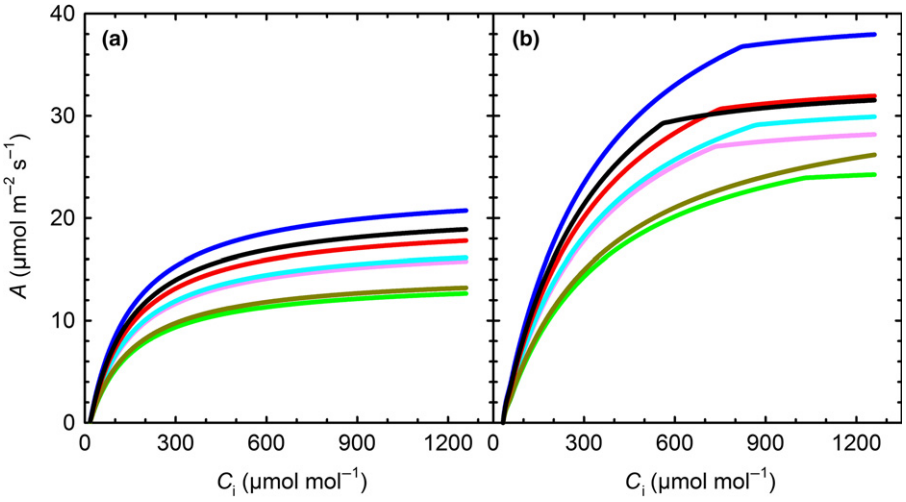

Fig. 3 Synthetic A–C_i curves modeled at 5°C (a) and 15°C (b). The response of photosynthesis (A) to rising intercellular CO_2 concentration (C_i) was modeled based on the data presented in Figs 1 and 2 and Eqns 1–3 for the seven species considered in this study: *Arctagrostis latifolia* (pink), *Dupontia fisheri* (green), *Arctophila fulva* (blue), *Carex aquatilis* (cyan), *Eriophorum angustifolium* (dark yellow), *Petasites frigidus* (red) and *Salix pulchra* (black).

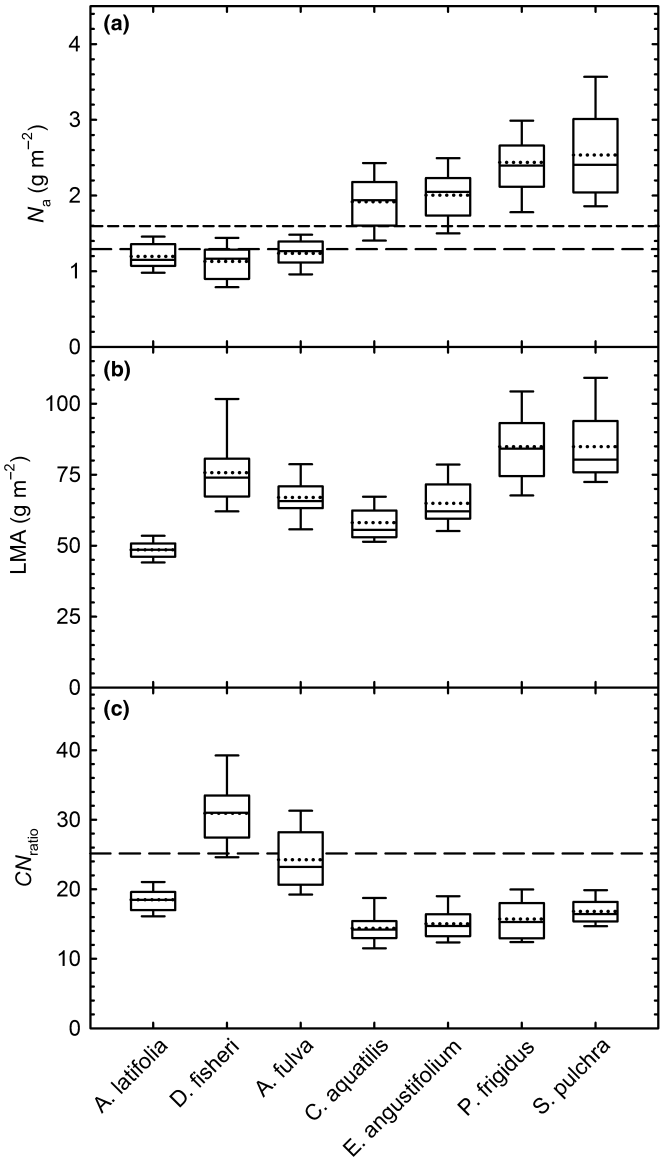

Fig. 4 Leaf nitrogen content (N_a, g m^{-2}, a), leaf mass area (LMA, g m^{-2}, b) and the ratio of leaf carbon to nitrogen content (CN_{ratio}, c). Data were collected in parallel with gas exchange in seven species located on the Barrow Environmental Observatory, Barrow Alaska. The broken lines in (a) indicate the mean value of N_a used by the Hybrid (short dashes) and Community Land Model (CLM) (long dashes) to parameterize the Arctic plant functional type (PFT). The broken line in (c) indicates the CN_{ratio} used by CLM to parameterize the Arctic PFT. Box plots show the interquartile range (box), median (solid line) and mean (broken line). The whiskers show the lowest and highest datum still within 1.5 × interquartile range of the lower and upper quartiles (n = 8–44 plants).

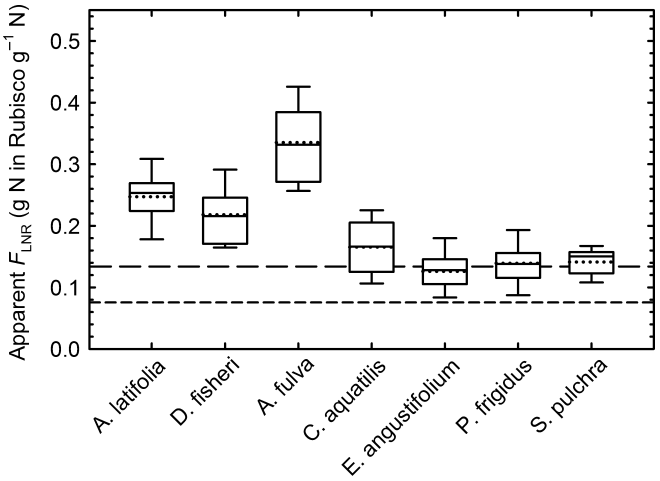

Fig. 5 The apparent fraction of leaf nitrogen invested in Rubisco (F_{LNR}) calculated using Eqn 5 from the data provided in Figs 2 and 4 and Rogers (2014). The broken lines show the value of F_{LNR} used in the Community Land Model (CLM) to parameterize the Arctic plant functional type (PFT, long dashes) and the F_{LNR} calculated for Hybrid based on N_a and $V_{c,max.25}$ in Table 1 (short dashes). Box plots show the interquartile range (box), median (solid line) and mean (broken line). The whiskers show the lowest and highest datum still within 1.5 × interquartile range of the lower and upper quartiles (n = 8–44 plants).

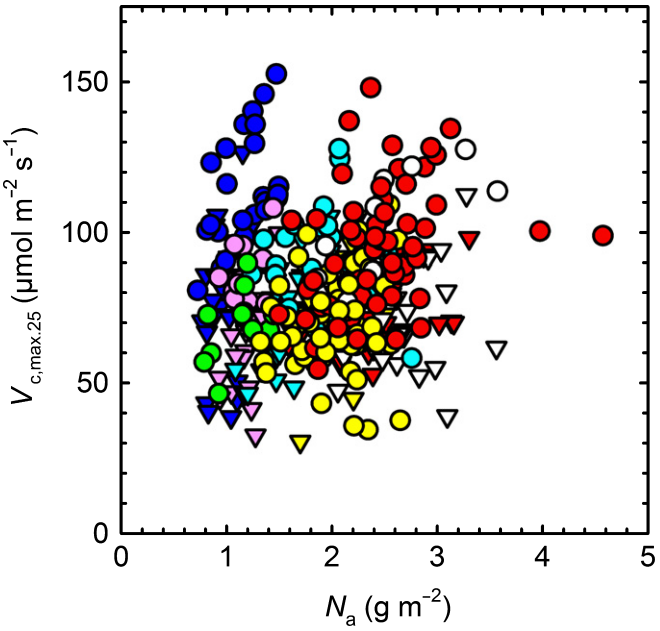

Fig. 6 Apparent maximum carboxylation rate scaled to 25°C ($V_{c,max.25}$) plotted against the area-based leaf nitrogen content (N_a). Estimates of apparent $V_{c,max.25}$ were scaled from gas exchange measurements made at growth temperature. These estimates were derived from A–C_i curves (circles) made between 2012 and 2015, and from steady-state, light-saturated photosynthesis using the one-point method made in 2016 (downward pointing triangles). Measurements were made on individual ramets of *Arctagrostis latifolia* (pink), *Dupontia fisheri* (green), *Arctophila fulva* (blue), *Carex aquatilis* (cyan), *Eriophorum angustifolium* (yellow), *Petasites frigidus* (red) and *Salix pulchra* (white) growing on the Barrow Environmental Observatory, Barrow, Alaska. No significant correlation was found.

Arctic midnight sun, and also to maximally exploit periods of high light on clear days during the short Arctic thaw season. In addition, many Arctic plants emerge from underneath the snow at the beginning of the growth season where temperatures are low, light levels are low and [CO_2] is typically elevated (Starr & Oberbauer, 2003; Saarinen *et al.*, 2016). Plants with a high investment in Rubisco and a high JV_{ratio} would be well adapted to exploit such conditions.

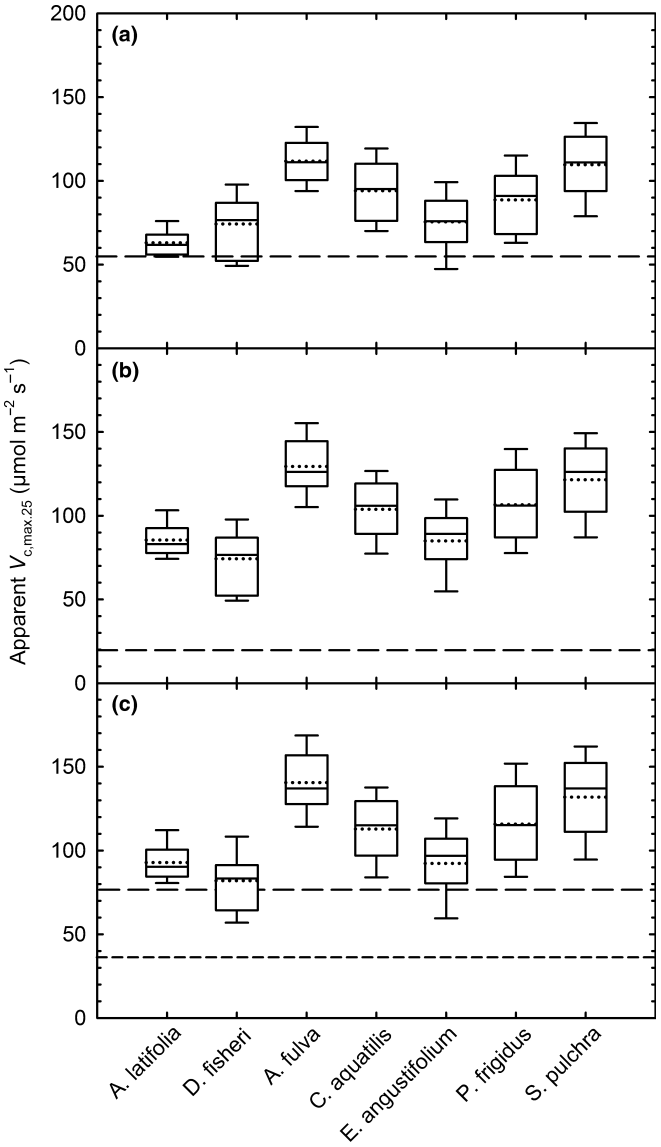

Fig. 7 Apparent maximum carboxylation rate measured at growth temperature and scaled to 25°C (apparent $V_{c,max.25}$) using the temperature response functions and parameterization associated with the four terrestrial biosphere models (TBMs) considered in this study (Table 1). The TBM model inputs are shown with a broken line: Atmosphere–Vegetation Interaction Model (AVIM) (a), Biosphere Energy Transfer Hydrology Scheme (BETHY) (b), Community Land Model (CLM) (long dashes, c) and Hybrid (short dashes, c). Gas exchange was measured in seven species located on the Barrow Environmental Observatory, Barrow, Alaska. Box plots show the interquartile range (box), median (solid line) and mean (broken line). The whiskers show the lowest and highest datum still within 1.5 × interquartile range of the lower and upper quartiles (n = 8–44 plants).

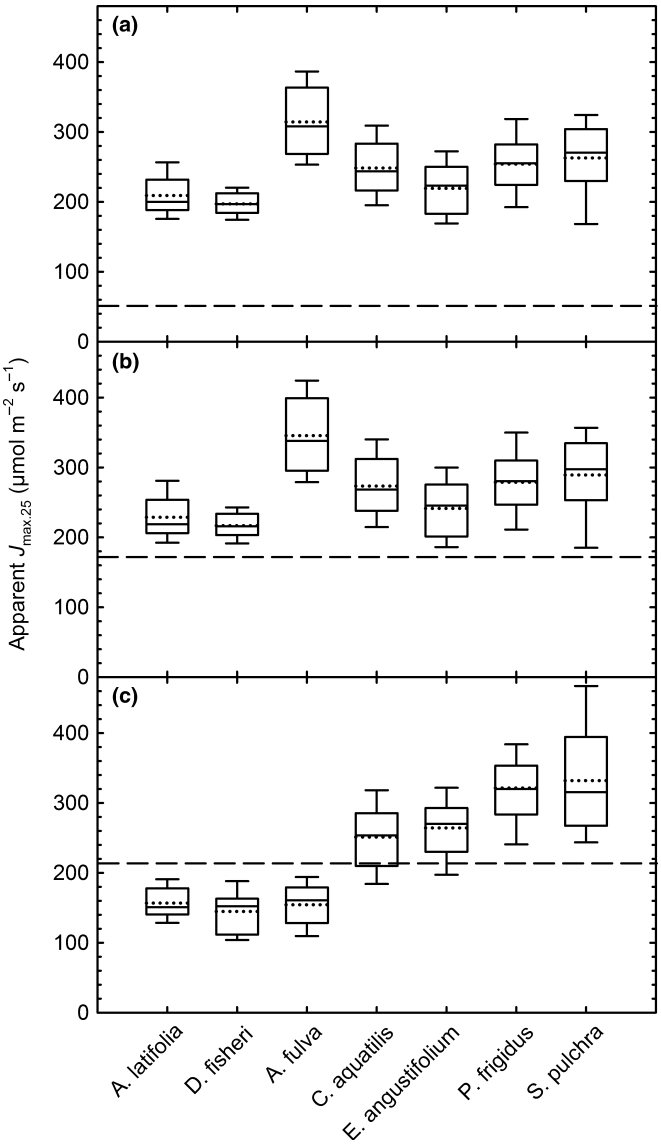

Fig. 8 Apparent maximum electron transport rate measured at growth temperature and scaled to 25°C (apparent $J_{max.25}$) using the temperature response functions, parameterization or the relationship with N_a (Hybrid), associated with three of the four terrestrial biosphere models (TBMs: Biosphere Energy Transfer Hydrology Scheme (BETHY), a; Community Land Model (CLM), b; Hybrid, c) considered in this study. The broken lines with long dashes in each panel indicate the TBM parameterization for the Arctic plant functional type (PFT). Gas exchange was measured in seven species located on the Barrow Environmental Observatory, Barrow, Alaska. Box plots show the interquartile range (box), median (solid line) and mean (broken line). The whiskers show the lowest and highest datum still within 1.5 × interquartile range of the lower and upper quartiles (n = 8–44 plants).

We observed a $JV_{ratio.25}$ (2.53) that is 28% higher than the $JV_{ratio.25}$ used by many models which do not account for temperature acclimation of photosynthesis (e.g. 1.97, Bonan *et al.*, 2011), highlighting the need for TBMs to account for thermal acclimation. Kattge & Knorr (2007) developed an approach to account for the acclimation of $JV_{ratio.25}$ to growth temperature, but their work did not include any measurements at which the growth temperature was below 10°C, and the data from boreal species in their study appeared to be outliers, exhibiting a markedly lower $JV_{ratio.25}$ than other species. This study adds new data at the low-temperature end of the synthesis by Kattge & Knorr (2007) and supports the relationship they presented, which is implemented in BETHY and CLM. However, the $JV_{ratio.25}$ observed here was still markedly higher than the value used in CLM, because CLM includes a lower limit for growth temperature of 11°C. This study suggests that, to more accurately

New Phytologist

Table 2 Modeled and measured light-saturated CO_2 assimilation at 5°C

Species/TBM	Modeled photosynthesis		Measured photosynthesis
	$V_{c,max.5}$ (μmol m^{-2} s^{-1})	A (μmol m^{-2} s^{-1})	A (μmol m^{-2} s^{-1})
Arctagrostis latifolia	17.9	11.2	9.2 ± 2.5
Dupontia fisheri	14.4	9.0	ND
Arctophila fulva	23.5	14.8	10.1 ± 1.8
Carex aquatilis	18.3	11.5	8.8 ± 1.9
Eriophorum angustifolium	15.0	9.4	10.1 ± 1.6
Petasites frigidus	20.2	12.7	11.3 ± 2.7
Salix pulchra	21.4	13.5	9.1 ± 2.5
Species mean	**18.6 ± 3.3**	**11.7 ± 2.1**	**9.8 ± 0.9**
AVIM	9.5	6.0	
BETHY	2.0	1.3	
CLM4.5	11.8	7.4	
Hybrid6.5	5.6	3.5	
Model mean	**7.2 ± 4.3**	**4.5 ± 2.7**	

Leaf-level CO_2 assimilation (A) modeled for the seven Arctic species in this study and for the Arctic plant functional types (PFT) represented in four terrestrial biosphere models (Table 1). Leaf-level, light-saturated A was modeled using Eqns 1–3, where leaf temperature = 5°C, CO_2 concentration = 390 μmol mol^{-1}, O_2 concentration = 210 mmol mol^{-1} and C_i : C_a ratio = 0.7. Under these conditions, photosynthesis was limited by carboxylation capacity. $V_{c,max.5}$ for the seven species was obtained by scaling $V_{c,max.25}$ (Fig. 2) to 5°C using Eqn 4 and the E_a values presented in Fig. 1. $V_{c,max.5}$ for the models was calculated by scaling $V_{c,max.25}$ for the Arctic PFT using the model-specific $V_{c,max.25}$ and temperature response function (TRF) (Table 1). Measured photosynthesis (n = 8–17 individual ramets per species, ± SD) was derived from a separate study on different plants in different locations on the Barrow Environmental Observatory (BEO), measured in a different year, where mean T_{leaf} = 5°C. Species and model means are shown ± SD. AVIM, Atmosphere–Vegetation Interaction Model; BETHY, Biosphere Energy Transfer Hydrology Scheme; CLM4.5, Community Land Model v.4.5; Hybrid6.5, Hybrid v.6.5; ND, no data; TBM, terrestrial biosphere model.

capture the $JV_{ratio.25}$ in Arctic species, this lower limit should be removed from the model formulation.

Our biochemical data revealed markedly different strategies for N partitioning in these seven Arctic species. Some species (*A. latifolia*, *D. fisheri* and *A. fulva*) had a tightly constrained N_a, whereas others, notably *S. pulchra* and *P. frigidus*, had a large range in N_a (Fig. 4), suggesting that N_a may drive the greater plasticity in photosynthetic capacity (Fig. 2). Most of the species had a low CN_{ratio} in comparison with the value used by CLM (Fig. 4c). This indicates that the high N_a in some Arctic species is caused, in part, by a higher investment in N per unit C, and not just a high N density per unit leaf area (Fig. 4). Our dataset afforded the opportunity to calculate apparent F_{LNR} for these Arctic species (a key model input for CLM), thus providing models with a parameter associated with N partitioning that could be used as a PFT-specific model input, or to evaluate prognostic N allocation models, e.g. Ali *et al.* (2016). It is notable that species with a lower N_a (*A. latifolia*, *D. fisheri* and *A. fulva*, Fig. 4) also had a high F_{LNR} (Fig. 5), suggesting that the high partitioning of N to Rubisco in these species enabled them to produce leaves with a lower N_a (Fig. 4), but comparable photosynthetic capacity (Fig. 2), which, at the whole-plant level, may enable a higher productivity for a given N supply.

One approach used by TBMs to derive $V_{c,max.25}$ is to use PFT-specific slopes and intercepts from the linear relationship with N_a (Medlyn *et al.*, 1999; Kattge *et al.*, 2009; Walker *et al.*, 2014). Previously, there was insufficient data to examine this relationship in Arctic species (Kattge *et al.*, 2009; Ziehn *et al.*, 2011). We did not observe a $V_{c,max.25}$–N_a relationship (Fig. 6). The different N allocation strategies outlined above, and the high diversity of leaf morphology in these species, may explain why we did not observe a $V_{c,max.25}$–N_a relationship at our field site, a finding also observed in *Betula nana* and *Eriophorum vaginatum* (van der Weg *et al.* 2013). Although data at the global or biome scale often demonstrate a strong relationship between $V_{c,max.25}$ and N_a (Kattge *et al.*, 2009; Walker *et al.*, 2014), these relationships can change markedly and even fall apart at finer scales (Feng & Dietze, 2013; Bahar *et al.*, 2016; Croft *et al.*, 2017), which has led to the use of other variables, including phosphorus, to explain global variation in $V_{c,max.25}$ (Walker *et al.*, 2014; Ali *et al.*, 2015; Croft *et al.*, 2017). There is evidence that phosphorus plays a role in limiting the productivity of Arctic tundra ecosystems, and may be a limiting nutrient on the coastal tundra in Barrow (Chapin *et al.*, 1975, 1995; Shaver & Chapin, 1980). However, the examination of N : phosphorus ratios across major biomes suggests that direct phosphorus limitation of photosynthesis in the Arctic is unlikely (Reich *et al.*, 2009).

As recently pointed out, it is critically important for models to make consistent use of kinetic constants and temperature response functions (Rogers *et al.*, 2017c). Therefore, the data presented here should be used in conjunction with the kinetic constants and temperature response functions associated with K_c, K_o and Γ* that are provided by Bernacchi *et al.* (2001). Similarly, use of the Arctic $V_{c,max.25}$ and $J_{max.25}$ data (Fig. 2) will require temperature scaling with the E_a values and the TRFs presented here (Fig. 1, Eqn 4). We also recognize that there are many alternative approaches to the analysis of photosynthetic CO_2 response curves, including, for example, those that use different TRFs, correct data for potential chamber leaks or account for mesophyll

conductance (Ethier & Livingston, 2004; Flexas *et al.*, 2007; Sharkey *et al.*, 2007; Gu *et al.*, 2010; Bernacchi *et al.*, 2013). To allow for future reanalysis of our data, and to maximize their further use by the modeling community, all of our data – including our raw gas exchange data – are available online (Rogers *et al.*, 2017a,b). In addition, we have submitted calculated photosynthetic parameters and biochemical trait data to the TRY database (Kattge *et al.*, 2011) and the database (www.BETYdb.org) associated with the Predictive Ecosystem Analyzer (PEcAn) project (Lebauer *et al.*, 2013).

In addition to advancing our understanding of photosynthesis in the Arctic, these data clearly indicate that CO_2 assimilation in Arctic vegetation is poorly represented by current TBMs. Although we caution that these data and insights are only from one site in the high Arctic, this study represents a significant advance, and we hope that the TBM community will improve the representation of CO_2 assimilation in the Arctic by using these data.

Acknowledgements

We are grateful for the technical assistance provided by Stefanie Lasota. This work was supported by the Next-Generation Ecosystem Experiments (NGEE Arctic) project which is supported by the Office of Biological and Environmental Research in the Department of Energy, Office of Science, and through the United States Department of Energy contract no. DE-SC0012704 to Brookhaven National Laboratory. The authors are grateful to UIC Science for logistical support.

Author contributions

A.R. designed the study with input from V.L.S., S.P.S. and S.D.W. The data were collected and analyzed by A.R., K.S.E. and S.P.S. The initial draft of the manuscript was prepared by A.R. All authors contributed to the writing.

References

Ainsworth EA, Davey PA, Hymus GJ, Osborne CP, Rogers A, Blum H, Nosberger J, Long SP. 2003. Is stimulation of leaf photosynthesis by elevated carbon dioxide concentration maintained in the long term? A test with *Lolium perenne* grown for 10 years at two nitrogen fertilization levels under Free Air CO_2 Enrichment (FACE). *Plant, Cell & Environment* **26**: 705–714.

Albert KR, Mikkelsen TN, Ro-Poulsen H, Arndal MF, Michelsen A. 2011. Ambient UV-B radiation reduces PSII performance and net photosynthesis in high Arctic *Salix arctica*. *Environmental and Experimental Botany* **73**: 10–18.

Ali AA, Xu C, Rogers A, Fisher RA, Wullschleger SD, Massoud EC, Vrugt JA, Muss JD, McDowell NG, Fisher JB *et al.* 2016. A global scale mechanistic model of photosynthetic capacity (LUNA V1.0). *Geoscientific Model Development* **9**: 587–606.

Ali AA, Xu CG, Rogers A, McDowell NG, Medlyn BE, Fisher RA, Wullschleger SD, Reich PB, Vrugt JA, Bauerle WL *et al.* 2015. Global-scale environmental control of plant photosynthetic capacity. *Ecological Applications* **25**: 2349–2365.

Alton PB. 2017. Retrieval of seasonal Rubisco-limited photosynthetic capacity at global FLUXNET sites from hyperspectral satellite remote sensing: impact on carbon modelling. *Agricultural and Forest Meteorology* **232**: 74–88.

Ardia D. 2009. *DEoptim: differential evolution optimization in R.* R package, version 1.3-3. http://CRAN.R-project.org/package=DEoptim.

Bahar NHA, Ishida FY, Weerasinghe LK, Guerrieri R, O'Sullivan OS, Bloomfield KJ, Asner GP, Martin RE, Lloyd J, Malhi Y *et al.* 2016. Leaf-level photosynthetic capacity in lowland Amazonian and high-elevation Andean tropical moist forests of Peru. *New Phytologist* **214**: 1002–1018.

Bernacchi CJ, Bagley JE, Serbin SP, Ruiz-Vera UM, Rosenthal DM, Vanloocke A. 2013. Modelling C_3 photosynthesis from the chloroplast to the ecosystem. *Plant, Cell & Environment* **36**: 1641–1657.

Bernacchi CJ, Leakey ADB, Heady LE, Morgan PB, Dohleman FG, McGrath JM, Gillespie KM, Wittig VE, Rogers A, Long SP *et al.* 2006. Hourly and seasonal variation in photosynthesis and stomatal conductance of soybean grown at future CO_2 and ozone concentrations for 3 years under fully open-air field conditions. *Plant, Cell & Environment* **29**: 2077–2090.

Bernacchi CJ, Morgan PB, Ort DR, Long SP. 2005. The growth of soybean under free air CO_2 enrichment (FACE) stimulates photosynthesis while decreasing *in vivo* Rubisco capacity. *Planta* **220**: 434–446.

Bernacchi CJ, Pimentel C, Long SP. 2003. *In vivo* temperature response functions of parameters required to model RuBP-limited photosynthesis. *Plant Cell and Environment* **26**: 1419–1430.

Bernacchi CJ, Singsaas EL, Pimentel C, Portis AR, Long SP. 2001. Improved temperature response functions for models of Rubisco-limited photosynthesis. *Plant, Cell & Environment* **24**: 253–259.

Bockheim JG, Everett LR, Hinkel KM, Nelson FE, Brown J. 1999. Soil organic carbon storage and distribution in Arctic Tundra, Barrow, Alaska. *Soil Science Society of America Journal* **63**: 934–940.

van Bodegom PM, Douma JC, Verheijen LM. 2014. A fully traits-based approach to modeling global vegetation distribution. *Proceedings of the National Academy of Sciences, USA* **111**: 13733–13738.

Boesgaard KS, Albert KR, Ro-Poulsen H, Michelsen A, Mikkelsen TN, Schmidt NM. 2012. Long-term structural canopy changes sustain net photosynthesis per ground area in high arctic *Vaccinium uliginosum* exposed to changes in near-ambient UV-B levels. *Physiologia Plantarum* **145**: 540–550.

Bonan GB, Lawrence PJ, Oleson KW, Levis S, Jung M, Reichstein M, Lawrence DM, Swenson SC. 2011. Improving canopy processes in the Community Land Model version 4 (CLM4) using global flux fields empirically inferred from FLUXNET data. *Journal of Geophysical Research–Biogeosciences* **116**: G02014.

Brown J, Everett KR, Webber PJ, Maclean SF, Murray DF. 1980. The coastal tundra at Barrow. In: Brown J, Miller PC, Tiezen LL, Bunnell FL, eds. *An Arctic ecosystem: the coastal tundra at Barrow, Alaska.* Stroudsburg, PA, USA: Dowden, Hutchinson & Ross, 1–29.

von Caemmerer S. 2000. *Biochemical models of leaf photosynthesis.* Collingwood, Australia: CSIRO Publishing.

Chapin FS, Bretharte MS, Hobbie SE, Zhong HL. 1996. Plant functional types as predictors of transient responses of arctic vegetation to global change. *Journal of Vegetation Science* **7**: 347–358.

Chapin FS, Shaver GR. 1996. Physiological and growth responses of arctic plants to a field experiment simulating climatic change. *Ecology* **77**: 822–840.

Chapin FS, Shaver GR, Giblin AE, Nadelhoffer KJ, Laundre JA. 1995. Response of Arctic tundra to experimental and observed changes in climate. *Ecology* **76**: 694–711.

Chapin FS, Van Cleve K, Tieszen LL. 1975. Seasonal nutrient dynamics of tundra vegetation at Barrow, Alaska. *Arctic and Alpine Research* **7**: 209–226.

Collatz GJ, Ball JT, Grivet C, Berry JA. 1991. Physiological and environmental regulation of stomatal conductance, photosynthesis and transpiration – a model that includes a laminar boundary layer. *Agricultural and Forest Meteorology* **54**: 107–136.

Croft H, Chen JM, Luo X, Bartlett P, Chen B, Staebler RM. 2017. Leaf chlorophyll content as a proxy for leaf photosynthetic capacity. *Global Change Biology* **23**: 3433–3964.

De Kauwe MG, Lin YS, Wright IJ, Medlyn BE, Crous KY, Ellsworth DS, Maire V, Prentice IC, Atkin OK, Rogers A *et al.* 2016. A test of the 'one-point method' for estimating maximum carboxylation capacity from field-measured, light-saturated photosynthesis. *New Phytologist* **210**: 1130–1144.

Dietze MC, Serbin SP, Davidson C, Desai AR, Feng X, Kelly R, Kooper R, LeBauer D, Mantooth J, McHenry K *et al.* 2014. A quantitative assessment of

a terrestrial biosphere model's data needs across North American biomes. *Journal of Geophysical Research-Biogeosciences* **119**: 286–300.

Dubois JJ, Fiscus BEL, Booker FL, Flowers MD, Reid CD. 2007. Optimizing the statistical estimation of the parameters of the Farquhar–von Caemmerer–Berry model of photosynthesis. *New Phytologist* **176**: 402–414.

Ethier GJ, Livingston NJ. 2004. On the need to incorporate sensitivity to CO_2 transfer conductance into the Farquhar–von Caemmerer–Berry leaf photosynthesis model. *Plant, Cell & Environment* **27**: 137–153.

Farquhar GD, Caemmerer SV, Berry JA. 1980. A biochemical model of photosynthetic CO_2 assimilation in leaves of C_3 species. *Planta* **149**: 78–90.

Feng XH, Dietze M. 2013. Scale dependence in the effects of leaf ecophysiological traits on photosynthesis: Bayesian parameterization of photosynthesis models. *New Phytologist* **200**: 1132–1144.

Fisher JB, Badgley G, Blyth E. 2012. Global nutrient limitation in terrestrial vegetation. *Global Biogeochemical Cycles* **26**: GB3007.

Fisher JB, Sikka M, Oechel WC, Huntzinger DN, Melton JR, Koven CD, Ahlstrom A, Arain MA, Baker I, Chen JM *et al.* 2014. Carbon cycle uncertainty in the Alaskan Arctic. *Biogeosciences* **11**: 4271–4288.

Fletcher BJ, Gornall JL, Poyatos R, Press MC, Stoy PC, Huntley B, Baxter R, Phoenix GK. 2012. Photosynthesis and productivity in heterogeneous arctic tundra: consequences for ecosystem function of mixing vegetation types at stand edges. *Journal of Ecology* **100**: 441–451.

Flexas J, Diaz-Espejo A, Berry JA, Cifre J, Galmes J, Kaidenhoff R, Medrano H, Ribas-Carbo M. 2007. Analysis of leakage in IRGA's leaf chambers of open gas exchange systems: quantification and its effects in photosynthesis parameterization. *Journal of Experimental Botany* **58**: 1533–1543.

Friedlingstein P, Cox P, Betts R, Bopp L, Von Bloh W, Brovkin V, Cadule P, Doney S, Eby M, Fung I *et al.* 2006. Climate-carbon cycle feedback analysis: results from the C^4MIP model intercomparison. *Journal of Climate* **19**: 3337–3353.

Friedlingstein P, Meinshausen M, Arora VK, Jones CD, Anav A, Liddicoat SK, Knutti R. 2014. Uncertainties in CMIP5 climate projections due to carbon cycle feedbacks. *Journal of Climate* **27**: 511–526.

Friend AD. 1995. PGEN – an integrated model of leaf photosynthesis, transpiration and conductance. *Ecological Modelling* **77**: 233–255.

Friend AD. 2010. Terrestrial plant production and climate change. *Journal of Experimental Botany* **61**: 1293–1309.

Friend AD, Kiang NY. 2005. Land surface model development for the GISS GCM: effects of improved canopy physiology on simulated climate. *Journal of Climate* **18**: 2883–2902.

Frost GV, Epstein HE. 2014. Tall shrub and tree expansion in Siberian tundra ecotones since the 1960s. *Global Change Biology* **20**: 1264–1277.

Galmes J, Hermida-Carrera C, Laanisto L, Niinemets U. 2016. A compendium of temperature responses of Rubisco kinetic traits: variability among and within photosynthetic groups and impacts on photosynthesis modeling. *Journal of Experimental Botany* **67**: 5067–5091.

Gu LH, Pallardy SG, Tu K, Law BE, Wullschleger SD. 2010. Reliable estimation of biochemical parameters from C_3 leaf photosynthesis-intercellular carbon dioxide response curves. *Plant, Cell & Environment* **33**: 1852–1874.

Heskel MA, Bitterman D, Atkin OK, Turnbull MH, Griffin KL. 2014. Seasonality of foliar respiration in two dominant plant species from the Arctic tundra: response to long-term warming and short-term temperature variability. *Functional Plant Biology* **41**: 287–300.

IPCC. 2013. Stocker TF, Qin D, Plattner G-K, Tignor M, Allen SK, Boschung J, Nauels A, Xia Y, Bex V, Midgley PM, eds. *Climate Change 2013: The Physical Science Basis. Contribution of Working Group I to the Fifth Assessment Report of the Intergovernmental Panel on Climate Change*. Cambridge, UK and New York, NY, USA: Cambridge University Press.

Iversen CM, Sloan VL, Sullivan PF, Euskirchen ES, McGuire AD, Norby RJ, Walker AP, Warren JM, Wullschleger SD. 2015. The unseen iceberg: plant roots in arctic tundra. *New Phytologist* **205**: 34–58.

James RA, Munns R, Von Caemmerer S, Trejo C, Miller C, Condon T. 2006. Photosynthetic capacity is related to the cellular and subcellular partitioning of Na^+, K^+ and Cl^- in salt-affected barley and durum wheat. *Plant, Cell & Environment* **29**: 2185–2197.

Jorgenson MT, Shur YL, Pullman ER. 2006. Abrupt increase in permafrost degradation in Arctic Alaska. *Geophysical Research Letters* **33**: L02503.

Kattge J, Diaz S, Lavorel S, Prentice C, Leadley P, Boenisch G, Garnier E, Westoby M, Reich PB, Wright IJ *et al.* 2011. TRY – a global database of plant traits. *Global Change Biology* **17**: 2905–2935.

Kattge J, Knorr W. 2007. Temperature acclimation in a biochemical model of photosynthesis: a reanalysis of data from 36 species. *Plant, Cell & Environment* **30**: 1176–1190.

Kattge J, Knorr W, Raddatz T, Wirth C. 2009. Quantifying photosynthetic capacity and its relationship to leaf nitrogen content for global-scale terrestrial biosphere models. *Global Change Biology* **15**: 976–991.

Kaufman DS, Schneider DP, McKay NP, Ammann CM, Bradley RS, Briffa KR, Miller GH, Otto-Bliesner BL, Overpeck JT, Vinther BM *et al.* 2009. Recent warming reverses long-term Arctic cooling. *Science* **325**: 1236–1239.

Koven CD, Schuur EAG, Schaedel C, Bohn TJ, Burke EJ, Chen G, Chen X, Ciais P, Grosse G, Harden JW *et al.* 2015. A simplified, data-constrained approach to estimate the permafrost carbon-climate feedback. *Philosophical Transactions of the Royal Society A: Mathematical Physical and Engineering Sciences* **373**: 20140423.

Kull O, Kruijt B. 1998. Leaf photosynthetic light response: a mechanistic model for scaling photosynthesis to leaves and canopies. *Functional Ecology* **12**: 767–777.

Lebauer DS, Wang D, Richter KT, Davidson CC, Dietze MC. 2013. Facilitating feedbacks between field measurements and ecosystem models. *Ecological Monographs* **83**: 133–154.

Leffler AJ, Welker JM. 2013. Long-term increases in snow pack elevate leaf N and photosynthesis in *Salix arctica*: responses to a snow fence experiment in the High Arctic of NW Greenland. *Environmental Research Letters* **8**: 025023.

Long SP, Bernacchi CJ. 2003. Gas exchange measurements, what can they tell us about the underlying limitations to photosynthesis? Procedures and sources of error. *Journal of Experimental Botany* **54**: 2393–2401.

Lu J, Ji J. 2006. A simulation and mechanism analysis of long-term variations at land surface over arid/semi-arid area in north China. *Journal of Geophysical Research-Atmospheres* **111**: D09306.

Medlyn BE, Badeck FW, De Pury DGG, Barton CVM, Broadmeadow M, Ceulemans R, De Angelis P, Forstreuter M, Jach ME, Kellomaki S *et al.* 1999. Effects of elevated CO_2 on photosynthesis in European forest species: a meta-analysis of model parameters. *Plant, Cell & Environment* **22**: 1475–1495.

Medlyn BE, Dreyer E, Ellsworth D, Forstreuter M, Harley PC, Kirschbaum MUF, Le Roux X, Montpied P, Strassemeyer J, Walcroft A *et al.* 2002. Temperature response of parameters of a biochemically based model of photosynthesis. II. A review of experimental data. *Plant, Cell & Environment* **25**: 1167–1179.

Muraoka H, Noda H, Uchida M, Ohtsuka T, Koizumi H, Nakatsubo T. 2008. Photosynthetic characteristics and biomass distribution of the dominant vascular plant species in a high Arctic tundra ecosystem, Ny-Ålesund Svalbard: implications for their role in ecosystem carbon gain. *Journal of Plant Research* **121**: 137–145.

Muraoka H, Uchida M, Mishio M, Nakatsubo T, Kanda H, Koizumi H. 2002. Leaf photosynthetic characteristics and net primary production of the polar willow (*Salix polaris*) in a high arctic polar semi-desert, Ny-Ålesund, Svalbard. *Canadian Journal of Botany–Revue Canadienne de Botanique* **80**: 1193–1202.

Oleson KW, Lawrence DM, Bonan GB, Drewniak B, Huang M, Koven CD, Levis S, Li F, Riley WJ, Subin ZM *et al.* 2013. *Technical description of version 4.5 of the community land model (CLM)*. Boulder, CO, USA: National Center for Atmospheric Research.

Patankar R, Mortazavi B, Oberbauer SF, Starr G. 2013. Diurnal patterns of gas-exchange and metabolic pools in tundra plants during three phases of the arctic growing season. *Ecology and Evolution* **3**: 375–388.

Price KV, Storn RM, Lampinen JA. 2006. *Differential evolution: a practical approach to global optimization*. New York, NY, USA: Springer.

R Development Core Team. 2013. *R: a language and environment for statistical computing*. Vienna, Austria: R Foundation for Statistical Computing. [WWW document] URL www.r-project.org [accessed October 2016].

Reich PB, Oleksyn J, Wright IJ. 2009. Leaf phosphorus influences the photosynthesis–nitrogen relation: a cross-biome analysis of 314 species. *Oecologia* **160**: 207–212.

Rogers A. 2014. The use and misuse of $V_{c,max}$ in Earth System Models. *Photosynthesis Research* **119**: 15–29.

Rogers A, Ely KS, Serbin SP. 2017a. *Leaf photosynthetic parameters V_{cmax} and J_{max} and supporting gas exchange data, Barrow, Alaska, 2012–2016. In: Next generation ecosystems experiment Arctic data collection.* Carbon Dioxide Information Analysis Center, Oak Ridge National Laboratory, Oak Ridge, TN, USA. [WWW document] URL doi: 10.5440/1336809 [accessed 1 January 2017].

Rogers A, Ely KS, Serbin SP, Lasota S, Liberman-Cribbin W. 2017b. *Leaf mass area, leaf carbon and nitrogen content, Barrow, Alaska, beginning 2012. In: Next generation ecosystems experiments Arctic data collection.* Carbon Dioxide Information Analysis Center, Oak Ridge National Laboratory, Oak Ridge, TN, USA. [WWW document] URL doi: 10.5440/1336812 [accessed 1 January 2017]. [Correction added after online publication 6 September 2017: the doi in Rogers *et al.* (2017b) has been corrected.]

Rogers A, Medlyn BE, Dukes JS, Bonan G, von Caemmerer S, Dietze MC, Kattge J, Leakey ADB, Mercado LM, Niinemets Ü *et al.* 2017c. A roadmap for improving the representation of photosynthesis in Earth system models. *New Phytologist* **213**: 22–42.

Saarinen T, Rasmus S, Lundell R, Kauppinen OK, Hanninen H. 2016. Photosynthetic and phenological responses of dwarf shrubs to the depth and properties of snow. *Oikos* **125**: 364–373.

Salmon VG, Soucy P, Mauritz M, Celis G, Natali SM, Mack MC, Schuur EAG. 2016. Nitrogen availability increases in a tundra ecosystem during five years of experimental permafrost thaw. *Global Change Biology* **22**: 1927–1941.

Sargsyan K, Safta C, Najm HN, Debusschere BJ, Ricciuto D, Thornton P. 2014. Dimensionality reduction for complex models via bayesian compressive sensing. *International Journal for Uncertainty Quantification* **4**: 63–93.

Schuur EAG, McGuire AD, Schaedel C, Grosse G, Harden JW, Hayes DJ, Hugelius G, Koven CD, Kuhry P, Lawrence DM *et al.* 2015. Climate change and the permafrost carbon feedback. *Nature* **520**: 171–179.

Schuur EAG, Vogel JG, Crummer KG, Lee H, Sickman JO, Osterkamp TE. 2009. The effect of permafrost thaw on old carbon release and net carbon exchange from tundra. *Nature* **459**: 556–559.

Serbin SP, Dillaway DN, Kruger EL, Townsend PA. 2012. Leaf optical properties reflect variation in photosynthetic metabolism and its sensitivity to temperature. *Journal of Experimental Botany* **63**: 489–502.

Sharkey TD. 1985. Photosynthesis in intact leaves of C_3 plants – physics, physiology and rate limitations. *Botanical Review* **51**: 53–105.

Sharkey TD, Bernacchi CJ, Farquhar GD, Singsaas EL. 2007. Fitting photosynthetic carbon dioxide response curves for C_3 leaves. *Plant, Cell & Environment* **30**: 1035–1040.

Shaver GR, Chapin FS. 1980. Response to fertilization by various plant-growth forms in an Alaskan tundra – nutrient accumulation and growth. *Ecology* **61**: 662–675.

Shaver GR, Chapin FS, Billings WD. 1979. Ecotypic differentiation in *Carex aquatilis* on ice-wedge polygons in the Alaskan coastal tundra. *Journal of Ecology* **67**: 1025–1046.

Shiklomanov NI, Streletskiy DA, Nelson FE, Hollister RD, Romanovsky VE, Tweedie CE, Bockheim JG, Brown J. 2010. Decadal variations of active-layer thickness in moisture-controlled landscapes, Barrow, Alaska. *Journal of Geophysical Research-Biogeosciences* **115**: G00104.

Smith NG, Dukes JS. 2013. Plant respiration and photosynthesis in global-scale models: incorporating acclimation to temperature and CO_2. *Global Change Biology* **19**: 45–63.

Souther S, Fetcher N, Fowler Z, Shaver GR, Mcgraw JB. 2014. Ecotypic differentiation in photosynthesis and growth of *Eriophorum vaginatum* along a latitudinal gradient in the Arctic tundra. *Botany-Botanique* **92**: 551–561.

Starr G, Neuman DS, Oberbauer SF. 2004. Ecophysiological analysis of two arctic sedges under reduced root temperatures. *Physiologia Plantarum* **120**: 458–464.

Starr G, Oberbauer SF. 2003. Photosynthesis of arctic evergreens under snow: implications for tundra ecosystem carbon balance. *Ecology* **84**: 1415–1420.

Sturm M, Racine C, Tape K. 2001. Climate change – increasing shrub abundance in the Arctic. *Nature* **411**: 546–547.

Tape K, Sturm M, Racine C. 2006. The evidence for shrub expansion in Northern Alaska and the Pan-Arctic. *Global Change Biology* **12**: 686–702.

Thornton PE, Zimmermann NE. 2007. An improved canopy integration scheme for a land surface model with prognostic canopy structure. *Journal of Climate* **20**: 3902–3923.

Torn M, Raz-Yaseef N, Billesbach D. 2014. *Eddy-covariance and auxiliary measurements, NGEE-Barrow, 2012–2013. Next generation ecosystem experiments – Arctic data collection.* Carbon Dioxide Information Analysis Center, Oak Ridge National Laboratory, Oak Ridge, TN, USA. [WWW document] URL doi: 10.5440/1124200 [accessed 8 January 2014].

Varhammar A, Wallin G, McLean CM, Dusenge ME, Medlyn BE, Hasper TB, Nsabimana D, Uddling J. 2015. Photosynthetic temperature responses of tree species in Rwanda: evidence of pronounced negative effects of high temperature in montane rainforest climax species. *New Phytologist* **206**: 1000–1012.

Walker AP, Beckerman AP, Gu LH, Kattge J, Cernusak LA, Domingues TF, Scales JC, Wohlfahrt G, Wullschleger SD, Woodward FI. 2014. The relationship of leaf photosynthetic traits – V_{cmax} and J_{max} – to leaf nitrogen, leaf phosphorus, and specific leaf area: a meta-analysis and modeling study. *Ecology and Evolution* **4**: 3218–3235.

van de Weg MJ, Shaver GR, Salmon VG. 2013. Contrasting effects of long term versus short-term nitrogen addition on photosynthesis and respiration in the Arctic. *Plant Ecology* **214**: 1273–1286.

Wookey PA, Robinson CH, Parsons AN, Welker JM, Press MC, Callaghan TV, Lee JA. 1995. Environmental constraints on the growth, photosynthesis and reproductive development of *Dryas octopetala* at a high Arctic polar semidesert, Svalbard. *Oecologia* **102**: 478–489.

Wullschleger SD. 1993. Biochemical limitations to carbon assimilation in C_3 plants – a retrospective analysis of the *A*/*Ci* curves from 109 species. *Journal of Experimental Botany* **44**: 907–920.

Wullschleger SD, Epstein HE, Box EO, Euskirchen ES, Goswami S, Iversen CM, Kattge J, Norby RJ, van Bodegom PM, Xu X. 2014. Plant functional types in Earth system models: past experiences and future directions for application of dynamic vegetation models in high-latitude ecosystems. *Annals of Botany* **114**: 1–16.

Xu CG, Fisher R, Wullschleger SD, Wilson CJ, Cai M, McDowell NG. 2012. Toward a mechanistic modeling of nitrogen limitation on vegetation dynamics. *PLoS ONE* **7**: e37914.

Zhu C, Ziska L, Zhu J, Zeng Q, Xie Z, Tang H, Jia X, Hasegawa T. 2012. The temporal and species dynamics of photosynthetic acclimation in flag leaves of rice (*Oryza sativa*) and wheat (*Triticum aestivum*) under elevated carbon dioxide. *Physiologia Plantarum* **145**: 395–405.

Ziehn T, Kattge J, Knorr W, Scholze M. 2011. Improving the predictability of global CO_2 assimilation rates under climate change. *Geophysical Research Letters* **38**: 10404.